ACS OMEGA

Open Access

http://pubs.acs.org/journal/acsodf

Article

A Novel Manganese Ion Delivery Carrier Promotes Immune Cell Proliferation and Enhances Innate Immune Responses

Lingjuan Wang,[§] Tingting Tang,[§] Kaiyue Zuo, Naiyu Liu, Yingrui Wei, and Xinjie Zhu*

Cite This: *ACS Omega* 2024, 9, 40226−40233

Read Online

ACCESS | Metrics & More | Article Recommendations | Supporting Information

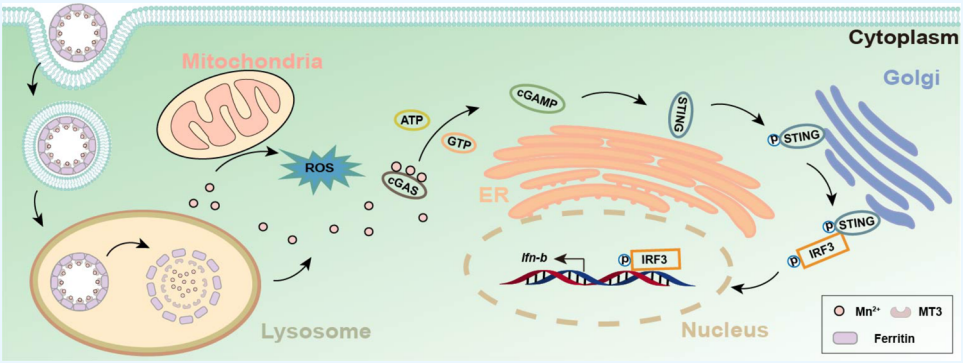

ABSTRACT: Manganese is a transition metal that is an essential trace element for human health. Manganese ions (Mn^{2+}), which serve as one of the most common transition metal ions, play vital roles in enhancing innate immune responses. However, immune agonists based on Mn^{2+} are poorly utilized in clinical trials due to poor chemodynamics and adverse events. In this work, we designed a novel delivery carrier for loading manganese ions by constructing hFn-MT3(Mn^{2+}) protein nanoparticles (termed as NPs(Mn^{2+})), which contained human ferritin heavy chain (hFn) and metallothionein-3 (MT3), induced by isopropyl β-D-thiogalactoside (IPTG) and manganese ions in the prokaryotic expression system. The NPs(Mn^{2+}) protein nanoparticles could not only stimulate immune cell proliferation but also activate innate immune responses via the cGAS-STING-IRF3 signaling pathway. Collectively, our results unveil a candidate strategy for delivering metal ions beyond Mn^{2+} and may broaden metal ion clinical use in the field of immunotherapies.

INTRODUCTION

Host immune responses, which serve as unique immune defense lines besides physical barriers, are important in protecting against foreign pathogens and strengthening the human body. Trace elements, which mainly involve iron (Fe), zinc (Zn), copper (Cu), manganese (Mn), chromium (Cr), selenium (Se), molybdenum (Mo), cobalt (Co), fluorine (F), etc., are essential for human health.[1,2] Trace element deficiencies are associated with aberrant morbidity and mortality.[3]

Recently, many studies have shown that transition metal ions can promote immune responses and exert antitumor efficacy.[4−8] Among them, manganese is a nutritional trace element required for a variety of physiological processes including antioxidant stress, development, and antitumor or antiviral functions.[9−14] Jiang and co-workers found that manganese ions were essential for the host to defend against DNA viruses.[15] However, manganese ions have a short half-life (only 1 min) that restricts their application to the windows in antitumor and antiviral therapies.[16] Thus, it is urgent to develop more effective manganese ion delivery carriers to enhance immune responses.

Drug delivery carriers based on nanotechnologies could not only change drug absorption, distribution, and metabolism in vivo but also achieve controlled drug release and hold the promise to promote therapeutic efficacy.[17−19] Human ferritin is a 24-polymer, whose outer and inner diameters are 12 and 8 nm, respectively, making it easy to accumulate in tumor regions through carrying drugs due to the enhanced permeability and retention (EPR) effect or transferrin receptor 1 (TFR1), which is overexpressed on tumor cell surfaces.[20−23] Yan and co-workers found that human ferritin (HFn) could be utilized as a nanocarrier to deliver encapsulated doxorubicin (Dox) through disassembling HFn in 8 M urea in the presence of Dox, followed by a reassembling process with a series of stepwise gradients of urea in PBS buffer,[24] traversing the blood−brain barrier and positively targeting glioma tumors via TFR1. However, the

Received: July 17, 2024
Revised: August 28, 2024
Accepted: September 4, 2024
Published: September 10, 2024

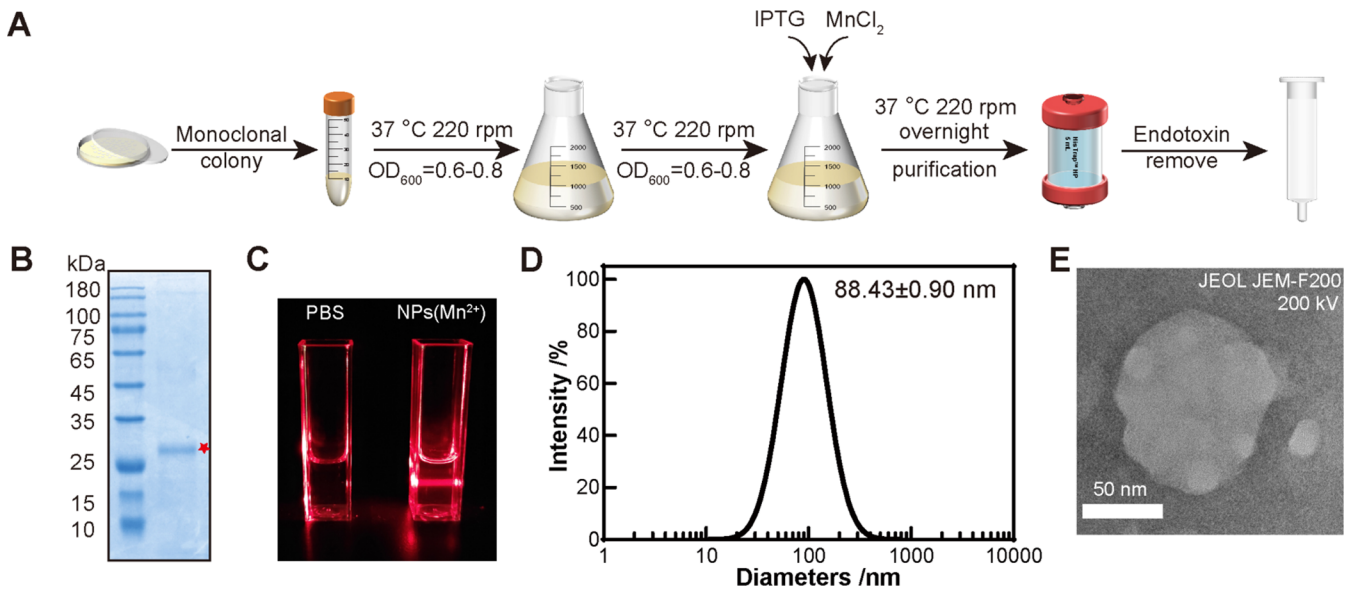

Figure 1. Protein expression and characterization of NPs(Mn^{2+}). (A) Schematic illustration of NPs(Mn^{2+}) expression and purification. (B) SDS-PAGE analysis of NPs(Mn^{2+}). (C) The Tyndall effect of NPs(Mn^{2+}). (D) The diameter analysis of NPs(Mn^{2+}). (E) Representative transmission electron microscopy images of NPs(Mn^{2+}).

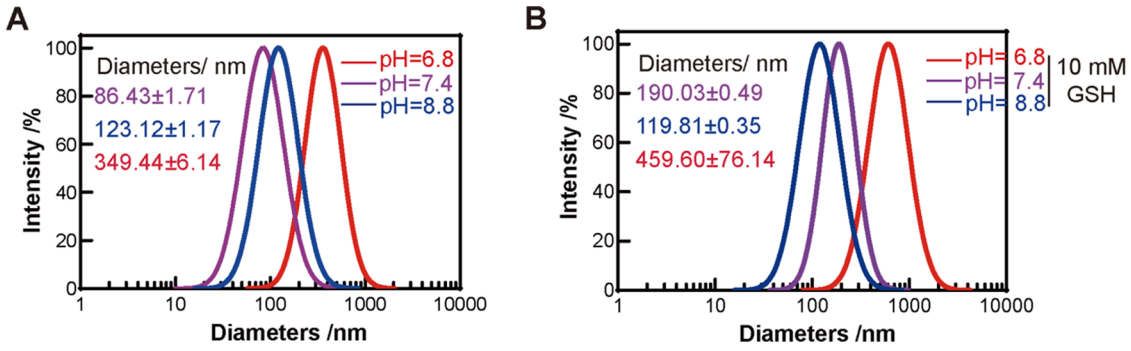

Figure 2. Diameters of NPs(Mn^{2+}) under circumstance. (A) Diameter changes of NPs(Mn^{2+}) in different pH solutions. (B) Diameter changes of NPs(Mn^{2+}) in different pH solutions containing 10 mM GSH.

processes have a great influence on protein activities and industrial manufactures.

In this study, we designed and constructed an hFn-MT3 fusion protein, spontaneously forming self-assembling nanoparticles (NPs(Mn^{2+})) that were concomitantly induced by IPTG and manganese ions during the expression process in *Escherichia coli*. The diameters of NPs(Mn^{2+}) were approximately 88.43 nm and would be changed in response to acidic or reduction circumstances. Moreover, NPs(Mn^{2+}) were located in the lysosome partially, promoting ROS production and cell proliferation for RAW 264.7 cells. Strikingly, the metal−protein nanoparticles could activate innate immune responses and initiate IFN-β secretion via the cGAS-STING-IRF3 signaling pathway. This work provides a new strategy for delivering manganese ions and enhancing innate immune responses.

RESULTS

Protein Expression and Characterization of NPs-(Mn^{2+}). Nanotechnologies have shown tremendous potential in drug deliveries and controllable release by carrying drug molecules to enhance antitumor or antiviral efficacy while alleviating adverse events.[4,25] Here, we selected human ferritin heavy chain (hFn) as a delivery carrier to transport manganese ions via fusing the MT3 domain (Figure S1). The expression and purification processes of hFn-MT3(Mn^{2+}) protein nanoparticles (termed as NPs(Mn^{2+})) are shown in Figure 1A. We performed the sodium dodecyl sulfate-polyacrylamide gel electrophoresis (SDS-PAGE) assay and liquid chromatography−mass spectrometry (LC-MS) to analyze its molecular weight. Consistent with theoretical molecular weight, the actual molecular weight for hFn-MT3 (Mn^{2+}) building blocks was approximately 30.35 kDa (Figures 1B and S2).

In addition, the clear Tyndall effect of the protein solution was observed, which provided strong evidence for proving the nanoscale of NPs(Mn^{2+}) (Figure 1C), possessing 88.43 ± 0.90 nm spherical nanoparticles, as revealed by dynamic light scattering (DLS) analysis and transmission electron microscopy (TEM) technology (Figure 1D,E).

To further analyze the stabilities of NPs(Mn^{2+}), we determined the diameter changes of NPs(Mn^{2+}) in acidic and reduction circumstances. The results showed that the diameter changes (ranging from 86.43 ± 1.71 to 349.44 ± 6.14 nm) were likely to be more sensitive in a microacidic solution (Figure 2A), and the diameters were scaled up to 459.60 ± 76.14 nm under stimulation with low pH (pH = 6.8) and 10 mM GSH (Figure 2B). Certainly, NPs(Mn^{2+}) had more stability, which could last

https://doi.org/10.1021/acsomega.4c06497
ACS Omega 2024, 9, 40226−40233

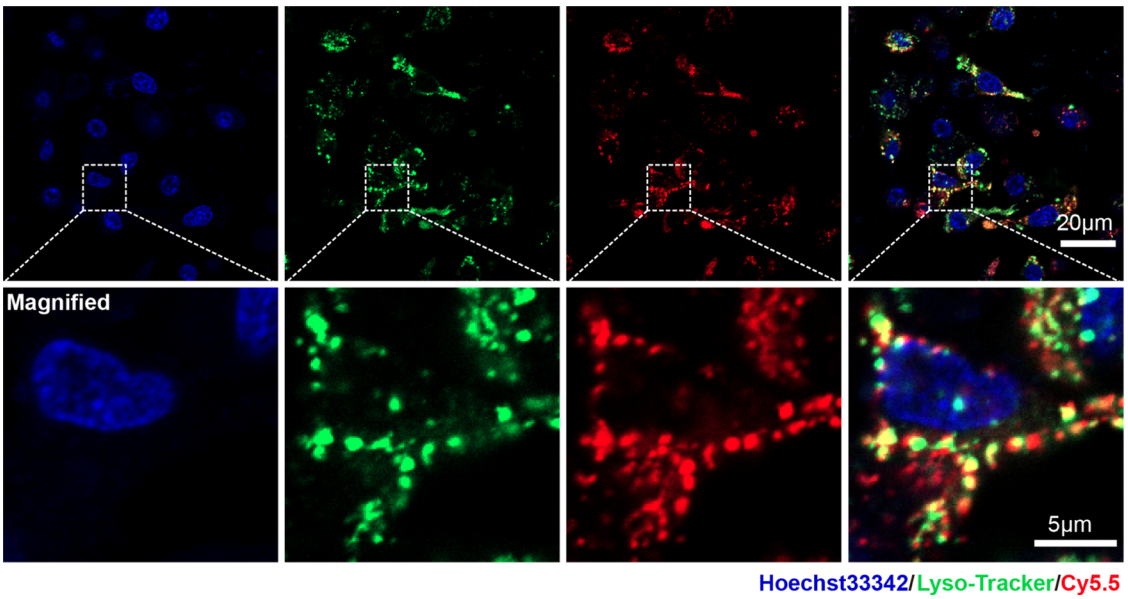

Figure 3. NPs(Mn^{2+}) localized in lysosomes partially. Representative fluorescence images of subcellular localization of NPs(Mn^{2+}). Cell nucleus, blue; lysosome, green; and NPs(Mn^{2+}), red.

for at least nearly 4 months at 4 °C compared to room temperature (Figure S3).

Localization of NPs(Mn^{2+}) in RAW 264.7 Cells. Lysosomes, which serve as the main digestion subcellular organelles, have emerged as multifunctional centers responsible for protein degradations or immune responses due to acidic circumstances and a variety of hydrolytic enzymes.[26] Generally, nanoscale substances are transported to lysosomes through an endocytosis pathway. Moon et al. reported that high-density lipoprotein-mimicking nanodiscs loaded with Dox were durably released from endosomes/lysosomes to trigger tumor immunogenic death and promote antitumor efficacy.[27] To explore NPs(Mn^{2+}) subcellular localization, the NPs(Mn^{2+}) were labeled with a Cy5.5 fluorescent molecule. As expected, the results showed that NPs(Mn^{2+}) could partially localize in lysosomes (Figures 3 and S4).

ROS Production and Cell Proliferation Induced by NPs(Mn^{2+}). Reactive oxygen species (ROS) represent a family of reactive molecules that arise during normal cellular metabolism and exert multiple biological functions rather than being viewed as just a toxic bypass product of mitochondrial respiration.[28,29] At modest levels, ROS are required to maintain normal homeostasis or modulate the signaling pathway through phosphorylation modification. Our previous studies have shown that the primary macrophage can be polarized toward the proinflammatory M1 macrophage under ROS stimulation, which inhibits viral replications.[30] In this work, we analyzed the ratio between Mn^{2+} and the hFn-MT3 monomer by inductively coupled plasma mass spectrometry (ICP-MS), and the results showed that its ratio was 1:2 (Figure S5). The NPs(Mn^{2+}) (100 μg/mL) were utilized to catalyze ROS production in RAW 264.7 cells. In contrast to NPs(Mn^{2+}), the equivalent NPs without loading transition manganese ions (Mn^{2+}) could not catalyze ROS production (Figure 4A−D). To verify the cytotoxicity of NPs(Mn^{2+}), RAW 264.7 cells were treated with NPs(Mn^{2+}) at different concentrations, showing that the NPs(Mn^{2+}) had no obvious cellular toxicity but promoted cell proliferation in vitro (Figure 4E).

Innate Immune Activation via the cGAS-STING Signaling Pathway. Manganese is essential for many biological processes in a manner that is dependent on innate immune responses. On the one hand, Mn^{2+} released by mitochondria and Golgi apparatus combines with cytosolic cyclic GMP−AMP synthase (cGAS), catalyzing the synthesis of the second messenger cyclic guanosine monophosphate adenosine monophosphate (cGAMP). On the other hand, Mn^{2+} enhanced the stimulator of interferon gene (STING) activity by augmenting cGAMP-STING binding affinity.[15,16,31−33] Taken together, the innate immune responses mediated by manganese ions are of paramount importance for antiviral or antitumor efficacies through the cGAS-STING signaling pathway.

To evaluate whether STING was involved in this signaling pathway, RAW 264.7 cells were treated with different concentrations of NPs(Mn^{2+}) for 24 h. It showed that the phosphorylation of STING and IRF3 (interferon regulate factor 3) was simultaneously upgraded in 100 μg/mL NPs(Mn^{2+}) (Figure 5A). Next, the RAW 264.7 cells were treated with 100 μg/mL NPs(Mn^{2+}) at different times. We found that the p-STING bands were upgraded in a time-dependent manner, and p-IRF3 reached the highest level in 2 h (Figure 5B). These data collectively elucidated that NPs(Mn^{2+}) are potent innate immune stimulators in vitro.

As the bridge of innate and adaptive immune responses, IFN-β was generated by p-IRF3 signaling transduction.[34−40] Consistent with STING/p-STING and IRF3/p-IRF3 signaling activation, the NPs(Mn^{2+}) (100 μg/mL) could initiate IFN-β secretion as high as 5-folds compared to other groups (Figure 5C). Intriguingly, the NPs(Mn^{2+}) were more sensitive to activating innate immune responses than the equivalent NPs without loading Mn^{2+} (Figure 5D).

To explore the roles of ROS that were produced through the Mn^{2+}-mediated Fenton-like reaction during innate immune responses, the ROS inhibitor N-acetyl cysteine (NAC) was utilized to inhibit ROS production. The results showed no significant changes in IFN-β levels between NPs(Mn^{2+}) and NPs(Mn^{2+}) with NAC (Figure 6). This elucidated that Mn^{2+} was essential for innate immune responses.

https://doi.org/10.1021/acsomega.4c06497
ACS Omega 2024, 9, 40226−40233

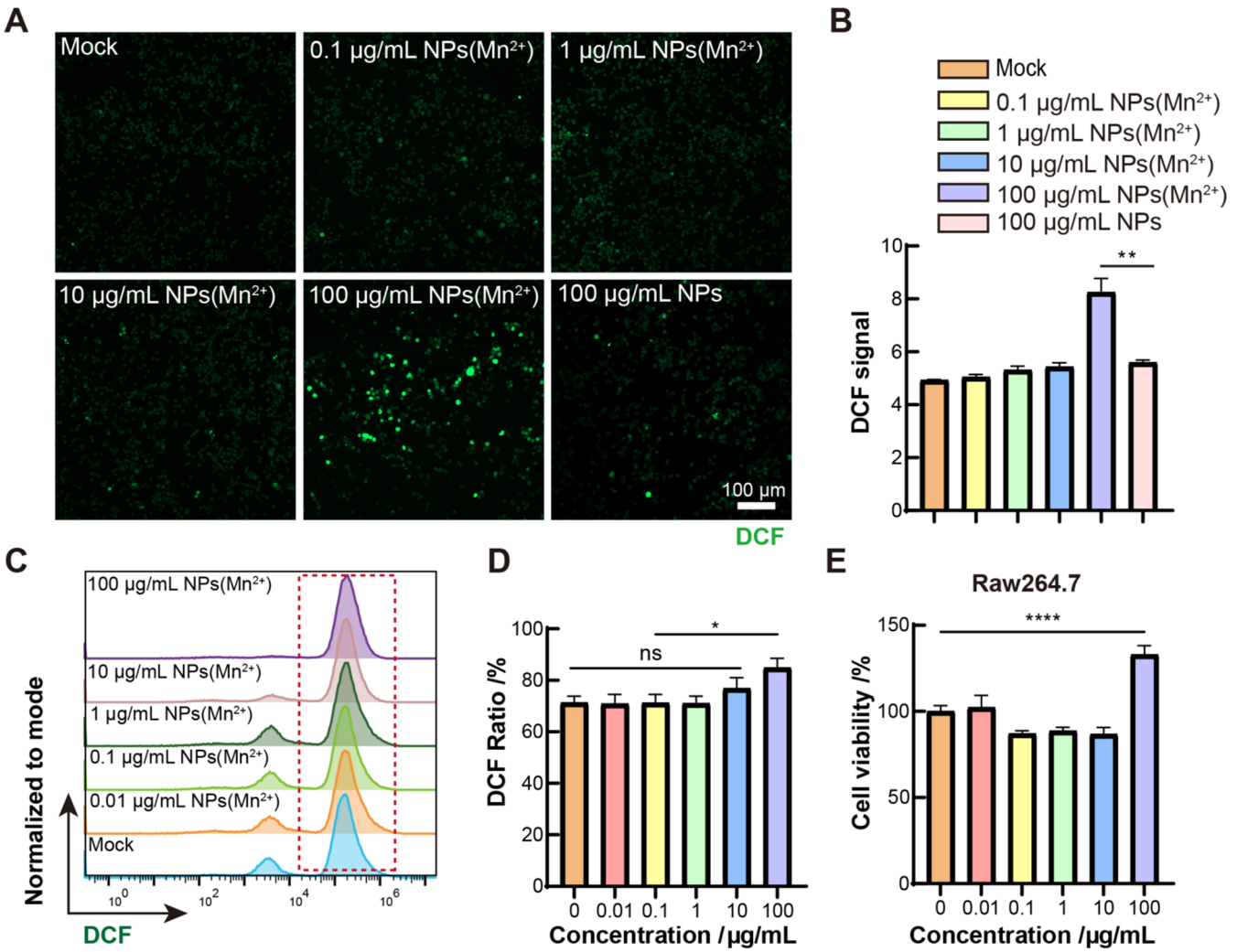

Figure 4. ROS production and cell proliferation induced by NPs(Mn^{2+}). (A, B) Representative fluorescence images (A) and relative intensities analysis (B) of ROS treated with NPs(Mn^{2+}) or NPs. (C, D) Flow cytometric qualitative (C) and quantification (D) analysis of ROS production treated with different concentrations of NP(Mn^{2+}). (E) Cell viability detection of RAW 264.7 cells treated with NPs(Mn^{2+}) at different concentrations for 24 h. Data are represented as means ± SEM (n = 3). ns, not significant; *p < 0.05; **p < 0.01; ****p < 0.0001.

DISCUSSION

As a promising antitumor therapeutic strategy, immunotherapies have shown tremendous potential in preventing and treating cancers by innate or adaptive immune responses. Nevertheless, approximately only 20% of tumor patients respond to immunotherapies due to low immune responses.[25,41] Therefore, how to enhance the immune responses remains a challenge.

In recent years, immunotherapies have achieved great breakthroughs in cancer therapies. Among them, the innate immune system, which serves as the first line of defense against cell carcinogenesis, plays vital roles in modulating immune responses. Zhang and colleagues reported BSA-templated MnO_2 nanosheets (SV@BMs), which conjugated 1 V209, a small molecule as a TLR7 agonist. SVN @BMs could react with GSH and release Mn^{2+}, which catalyzed ROS production via Mn^{2+}-induced Fenton-like reactions in macrophages. On the other hand, the primary macrophage could be polarized into the M1 macrophage, which promoted proinflammatory cytokine production and enhanced immunotherapeutic efficacies.[42] Meanwhile, Jiang and co-workers elucidated that bivalent manganese (Mn^{2+}) was critical for antiviral or antitumor immune responses through the cGAS-STING signaling pathway.[15,16] However, the inorganic manganese ions involved in these strategies have an extremely short half-life in vivo. Therefore, it is still a great challenge to develop a simple but efficient drug delivery carrier that enables loaded manganese ions and facilitates immune responses.

In this work, we designed and constructed protein nanoparticles (NPs(Mn^{2+})), which contained the hFn domain and bivalent manganese ions. The NPs(Mn^{2+}) could catalyze ROS production, promote cell proliferation, and activate innate immune responses in vitro, paving the way for multifunctional metal−protein nanodrug delivery carriers that are utilized for immunotherapies. However, there are still two aspects that remain to be explored. First, whether the NPs(Mn^{2+}) have antitumor efficacy in vivo. Second, whether there is another molecular mechanism for immune responses besides innate immune responses that are involved in the cGAS-STING signaling pathway. It will be of interest to explore these potential mechanisms in the future.

https://doi.org/10.1021/acsomega.4c06497
ACS Omega 2024, 9, 40226−40233

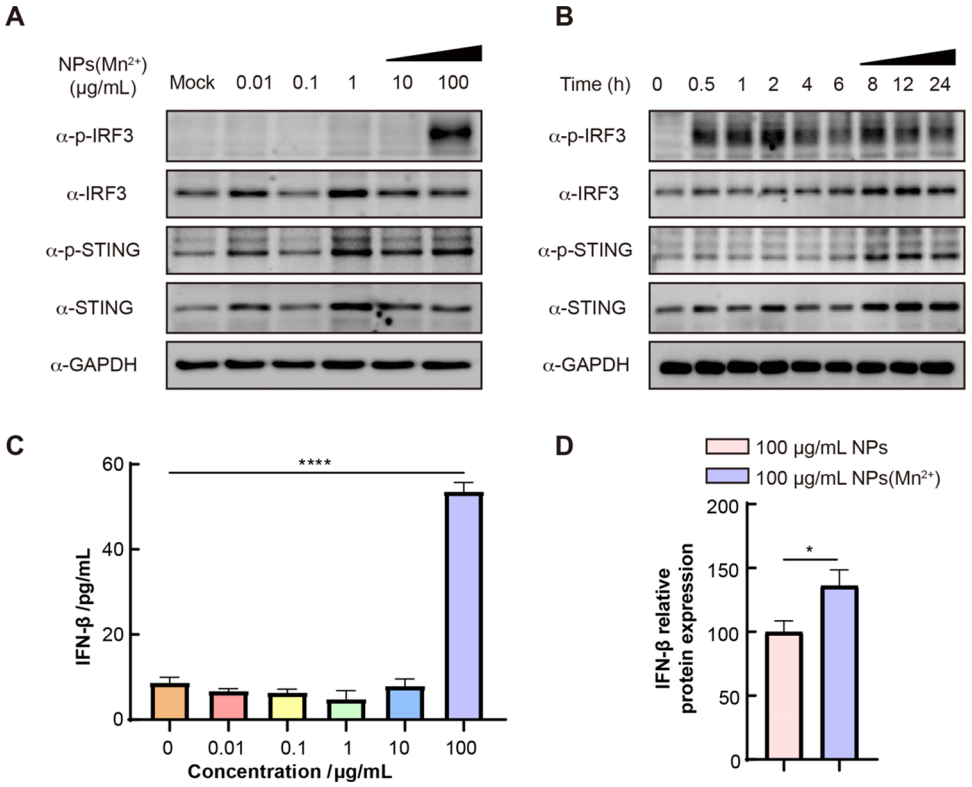

Figure 5. Innate immune activation via the cGAS-STING signaling pathway stimulated with NPs(Mn^{2+}). (A) Western blot analysis of STING/p-STING and IRF3/p-IRF3 in RAW 264.7 cells treated with different concentrations of NPs(Mn^{2+}) for 24 h. (B) Western blot analysis of STING/p-STING and IRF3/p-IRF3 in RAW 264.7 cells at different time points after being stimulated with 100 μg/mL NPs(Mn^{2+}). (C) Enzyme-linked immunosorbent assay (ELISA) of the secreted IFN-β protein expression level in the supernatant of RAW 264.7 cells treated with different concentrations of NPs(Mn^{2+}) for 24 h. (D) IFN-β relative protein expression level in the supernatant of RAW 264.7 cells treated with 100 μg/mL NPs(Mn^{2+}) and 100 μg/mL NPs. Data are represented as mean ± SEM (n = 3). *p < 0.05; ****p < 0.0001.

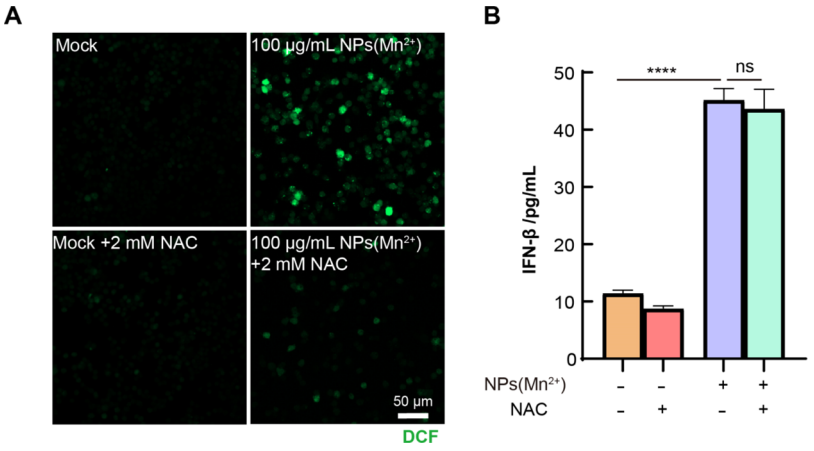

Figure 6. Mn^{2+} was essential for innate immune responses. (A) Representative fluorescence images of ROS treated with NPs(Mn^{2+}) or NPs(Mn^{2+}) plus NAC. (B) Enzyme-linked immunosorbent assay (ELISA) of secreted IFN-β in the supernatant of RAW 264.7 cells treated with NPs(Mn^{2+}) or NPs(Mn^{2+}) plus NAC for 24 h. ns, not significant; ****p < 0.0001.

CONCLUSIONS

In summary, we designed and constructed the recombinant protein hFn-MT3 that was loaded with bivalent manganese ions (Mn^{2+}). The NPs(Mn^{2+}) could catalyze ROS production via a Mn^{2+}-mediated Fenton-like reaction, promote cell proliferation, and enhance innate immune responses through the cGAS-STING-IRF3 signal pathway. The results indicated that metal-based protein nanoparticles are the potential prospect to enhance immune responses, improve the therapeutic benefits of metal immunotherapy, and widely broaden applications of manganese ions in immunotherapeutic fields.

MATERIALS AND METHODS

Materials. *E. coli* BL21(DE3) cells (CD-601-02) were purchased from Beijing TransGen Biotech Co., Ltd. Isopropyl β-D-thiogalactoside (IPTG) (BS119) was purchased from Biosharp. Phenylmethanesulfonylfluoride (PMSF, P8340) and RIPA (R0010) were purchased from Beijing Solarbio Science

https://doi.org/10.1021/acsomega.4c06497
ACS Omega 2024, 9, 40226−40233

&Technology Co., Ltd. A ToxinSensor Chromogenic LAL Endotoxin Assay Kit (L00350) was purchased from GenScript. DCFH-DA (D837204) was purchased from Shanghai Macklin Biochemical Technology Co., Ltd. RAW 264.7 cells (CL-0190) were purchased from Procell Life Science &Technology Co., Ltd. A HisTrap HP column (17524802) was purchased from Cytiva. A Pierce BCA Protein Assay Kit (BCA, 23227) was purchased from Thermo Scientific. LysoTracker Green (C1047) and Hoechst33342 (C1022) were purchased from Beyotime Biotechnology. The following antibodies were acquired from Cell Signaling Technology: GAPDH (14C10) Rabbit mAb (#2118), STING (D2P2F) Rabbit mAb (#13647), Phospho-STING (Ser365) (D8F4W) Rabbit mAb (#72971), IRF-3 (D83B9) Rabbit mAb (#4302), and Phospho-IRF-3 (Ser396) (4D4G) Rabbit mAb (#4947). HRP AffiniPure Goat anti-Rabbit lgG (H + L) was purchased from EarthOx (E030120). The following reagents were purchased from Mei5 Biotechnology Co., Ltd.: M5 HiClear Prestained Protein Ladder (10−180 kDa) (MF212), M5 HiPer Phosphatase Inhibitor Cocktail 1 (100× in DMSO) (MF675) and 2 (100× in ddH_2O) (MF676), M5 Protease Inhibitor Cocktail (100×) (MF182), and M5 HiPer ECL Western HRP Substrate (MF074). A Mouse IFN-β ELISA Kit (CME0116) was purchased from Suzhou 4A Biotech Co., Ltd.

NPs(Mn^{2+}) Protein Nanoparticle Expression and Purification. The procedure was described in a previous study.[30] Briefly, DNA sequences of 6× His-tagged hFn-MT3 were cloned to pET28a (+). The plasmid was transformed into BL21(DE3) competent *E. coli* cells. A single clone was picked and cultured in 10 mL of the lysogeny broth medium (LB) with 100 μg/mL kanamycin at 37 °C for 5 h while shaking until OD_{600} reached 0.6−0.8 approximately. The bacteria were amplified in 1 L of LB with kanamycin at 37 °C and shaken for 4 h until OD_{600} reached 0.6−0.8 again. Bacteria solution was added with 1 mM isopropylthiogalactoside (IPTG) and $MnCl_2$ to induce protein expression overnight at 37 °C. The protein-expressing bacteria were harvested and lysed by sonication. The lysate supernatants were purified with a HisTrap HP column to enrich His-tagged NPs(Mn^{2+}), followed by protein elution with imidazole (250 mM). The purified protein was determined by SDS-PAGE on 12% polyacrylamide gel. Afterward, the gel was stained with Coomassie staining solution and analyzed through Bio-Rad ChemiDoc XRS^+ software.

Before performing all assays, endotoxin affinity agarose was used to remove the endotoxin from all proteins. The final concentration of endotoxin was measured by a Chromogenic LAL Endotoxin Assay Kit. The results showed that the endotoxin was less than 0.025 EU/mL, significantly below the safety limit required of medical devices and parenteral drugs (0.5 EU/mL according to the FDA of U.S.A.).

DLS Measurement. The diameters of NPs(Mn^{2+}) in different circumstances were determined using a Nano 90Plus PALS analyzer device (Brookhaven, USA). The measurements were made by diluting the NPs(Mn^{2+}) with 1 mL of solutions with different pH values ranging from 6.8 to 8.8 containing 10 mM GSH or not. The Tyndall effect was observed by red laser light irradiation.

TEM Observation. The NPs(Mn^{2+}) protein nanoparticles were centrifuged to remove salt and resuspended with purified water, and then 10 μL of desalted NPs(Mn^{2+}) protein nanoparticles were dropped onto a carbon-shadowed copper grid, allowed to dry naturally, and dyed with 1% phosphotungstic acid. A field emission transmission electron microscope (JEOL, JEM-F200) operating at 200 kV was used to observe the morphology of NPs(Mn^{2+}).

Localization of NPs(Mn^{2+}) Protein Nanoparticles in RAW 264.7 Cells. Before fluorescence imaging, the NPs(Mn^{2+}) protein nanoparticles were labeled with Cy5.5 fluorescent molecules to obtain NPs(Mn^{2+})−Cy5.5. RAW 264.7 cells were cultured in $DMEM^{+2}$ in a confocal chamber at 37 °C in a 5% CO_2 incubator (6 × 10^5 cells). NPs(Mn^{2+})−Cy5.5 was added for 6 h. The cells were washed twice with PBS and then incubated in LysoTracker for 30 min at 37 °C and 5% CO_2. The cells were washed twice with PBS and stained with Hoechst33342 (1:500) for 15 min. The cells were washed twice again before imaging for laser scanning confocal microscopy (LSCM).

Determination of ROS. For flow cytometric analysis, RAW 264.7 cells were cultured in a 6-well plate (2 × 10^6 cells) for 24 h and treated with different concentrations of NPs(Mn^{2+}) protein nanoparticles for 24 h. The cell culture medium was removed completely, and 2 mL of DCFH-DA (5 μM) was added to each well. The cells were incubated at 37 °C in the dark with a 5% CO_2 incubator for 30 min and then were washed 3 times with PBS to remove free DCFH-DA. The cells were collected in a 1.5 mL EP tube and analyzed by flow cytometry (BD, C6 plus). For observation of fluorescence images, the steps were the same as above. The only difference was that the treated cells were visualized directly by LSCM (Zeiss, LSM900).

Cell Proliferation Assay. The effect of NPs(Mn^{2+}) protein nanoparticles on cell proliferation for RAW 264.7 cells was performed using a CCK-8 Kit. Different concentrations of NPs(Mn^{2+}) protein nanoparticles were added to each well (24-well plate, 5 × 10^5 cells/well) and incubated for 24 h. 50 μL of CCK-8 solution was added to each well. After incubation for 1 h, OD_{450} was determined with a multimode microplate reader (SpectraMax i3x).

Western Blot. RAW 264.7 cells were cultured in a 6-well plate and treated with NPs(Mn^{2+}) protein nanoparticles in different manners that belonged to dose-dependence or time-dependence. The cells were harvested and lysed with RIPA buffer containing phosphatase and protease inhibitors. The supernatants were collected for concentration measurement using a BCA Kit. Then, every sample (10 μg (10 μL) of total protein/well) was boiled for 10 min at 98 °C and short centrifuged at 4 °C with maximum speed.

The boiled samples were subjected to SDS-PAGE protein electrophoresis using 12% polyacrylamide gel. Gels were run at 80 V for 30 min, then changed to 120 V for 90 min, and subsequently transferred to PVDF membranes. The membranes were blocked with 5% BSA (PBST) for 1 h at room temperature, then washed three times with 0.1% PBST, and incubated into the corresponding primary antibody (1:1000 dilution) overnight at 4 °C on a shaker. After washing with PBST three times, the membranes were incubated with the corresponding secondary antibody (1:5000) for 90 min at room temperature. The membrane was washed three times in 0.1% PBST at room temperature and developed with the ECL substrate. The images were visualized by a ChemiDoc XRS^+ Gel Imaging System (BIO-RAD).

Enzyme-Linked Immunosorbent Assay. RAW 264.7 cells were cultured in 12-well plates (1 × 10^6 cells) and treated with corresponding drugs for 24 h. The cell supernatant was centrifuged at 4 °C for 10 min with maximum speed and then collected in 1.5 mL EP tubes. IFN-β was measured by ELISA kits according to the manufacturer's instructions.

https://doi.org/10.1021/acsomega.4c06497
ACS Omega 2024, 9, 40226−40233

Statistical Analysis. The data shown were representative of three independent experiments at least. The results of western blotting were displayed by Image Lab. The statistical analysis was done using GraphPad Prism 9 and figures were generated by Adobe Illustrator 2021. Results were expressed as means ± SEM. Unless specifically noted, differences between two groups were compared by unpaired Student's *t*-test, and P values of less than 0.05 were considered significant. ns, not significant; $*p < 0.05$; $**p < 0.01$; $***p < 0.001$; $****p < 0.0001$.

■ ASSOCIATED CONTENT

Supporting Information

The Supporting Information is available free of charge at https://pubs.acs.org/doi/10.1021/acsomega.4c06497.

DNA and protein sequences of the hFn-MT3(Mn^{2+}) fusion protein; mass spectra of the NPs(Mn^{2+}) monomer; stability of NPs(Mn^{2+}) detected by DLS under 4 °C or room temperature; Pearson's correction coefficient analysis for co-localization between the lysosome and NPs(Mn^{2+}); and inductively coupled plasma mass spectrometry (ICP-MS) analysis for manganese ion detection in NPs(Mn^{2+}) (PDF)

■ AUTHOR INFORMATION

Corresponding Author

Xinjie Zhu − *Key Laboratory of Tropical Biological Resources of Ministry of Education, School of Pharmaceutical Sciences, Hainan University, Haikou 570228, China; Li Song's Academician Workstation of Hainan University (School of Pharmaceutical Sciences), Hainan University, Sanya 572000, China;* orcid.org/0009-0004-3502-9329; Email: zhuxj@hainanu.edu.cn

Authors

Lingjuan Wang − *Key Laboratory of Tropical Biological Resources of Ministry of Education, School of Pharmaceutical Sciences, Hainan University, Haikou 570228, China; Li Song's Academician Workstation of Hainan University (School of Pharmaceutical Sciences), Hainan University, Sanya 572000, China*

Tingting Tang − *Key Laboratory of Tropical Biological Resources of Ministry of Education, School of Pharmaceutical Sciences, Hainan University, Haikou 570228, China; Li Song's Academician Workstation of Hainan University (School of Pharmaceutical Sciences), Hainan University, Sanya 572000, China*

Kaiyue Zuo − *Key Laboratory of Tropical Biological Resources of Ministry of Education, School of Pharmaceutical Sciences, Hainan University, Haikou 570228, China; Li Song's Academician Workstation of Hainan University (School of Pharmaceutical Sciences), Hainan University, Sanya 572000, China*

Naiyu Liu − *Key Laboratory of Tropical Biological Resources of Ministry of Education, School of Pharmaceutical Sciences, Hainan University, Haikou 570228, China; Li Song's Academician Workstation of Hainan University (School of Pharmaceutical Sciences), Hainan University, Sanya 572000, China*

Yingrui Wei − *Key Laboratory of Tropical Biological Resources of Ministry of Education, School of Pharmaceutical Sciences, Hainan University, Haikou 570228, China; Li Song's Academician Workstation of Hainan University (School of Pharmaceutical Sciences), Hainan University, Sanya 572000, China*

Complete contact information is available at: https://pubs.acs.org/10.1021/acsomega.4c06497

Author Contributions

[§]L.W. and T.T. authors contributed equally to this work and are cofirst authors. L.W., T.T., and X.Z. conceived and designed the idea of the present work. L.W., T.T., K.Z., N.L., and Y.W. performed experiments and analyzed the data. L.W. wrote the manuscript and X.Z. revised it. All authors read and approved the final manuscript.

Notes

The authors declare no competing financial interest.

■ ACKNOWLEDGMENTS

This work was supported by Fundamental Research Funds for Hainan University (KYQD(ZR)-21109) and Hainan Provincial Natural Science Foundation of China (Grant No. 824QN246). The authors would like to thank the Institutional Center for Shared Technologies and Facilities of IDSSE, CAS for Research Assistant Dongmei Wang and Pingjing Li. The authors thank Yuan Xue and Long Chen (Peking University) for support with ChemDraw and Adobe Illustrator software.

■ REFERENCES

(1) Zoroddu, M. A.; Aaseth, J.; Crisponi, G.; Medici, S.; Peana, M.; Nurchi, V. M. The essential metals for humans: a brief overview. *J. Inorg. Biochem.* **2019**, *195*, 120−129.

(2) Nordberg, M.; Nordberg, G. F. Trace element research-historical and future aspects. *J. Trace Elem. Med. Biol.* **2016**, *38*, 46−52.

(3) Zemrani, B.; Bines, J. E. Recent insights into trace element deficiencies: causes, recognition and correction. *Curr. Opin. Gastroenterol.* **2020**, *36* (2), 110−117.

(4) Wang, C.; Zhang, R.; Wei, X.; Lv, M.; Jiang, Z. Metalloimmunology: The metal ion-controlled immunity. *Adv. Immunol.* **2020**, *145*, 187−241.

(5) Zhang, L.; Zhao, J.; Hu, X.; Wang, C.; Jia, Y.; Zhu, C.; Xie, S.; Lee, J.; Li, F.; Ling, D. A Peritumorally Injected Immunomodulating Adjuvant Elicits Robust and Safe Metalloimmunotherapy against Solid Tumors. *Adv. Mater.* **2022**, *34* (41), No. e2206915.

(6) Yan, J.; Wang, G.; Xie, L.; Tian, H.; Li, J.; Li, B.; Sang, W.; Li, W.; Zhang, Z.; Dai, Y. Engineering Radiosensitizer-Based Metal-Phenolic Networks Potentiate STING Pathway Activation for Advanced Radiotherapy. *Adv. Mater.* **2022**, *34* (10), No. e2105783.

(7) Oluwole, S. A.; Weldu, W. D.; Jayaraman, K.; Barnard, K. A.; Agatemor, C. Design Principles for Immunomodulatory Biomaterials *ACS Appl. Bio Mater.* 2024 DOI: 10.1021/acsabm.4c00537.

(8) Paul, V. J.; Sharma, P.; Shanavas, A. Self-Assembled Nanobiomaterials for Combination Immunotherapy. *ACS Appl. Bio Mater.* **2023**, *7* (8), 4962−4674, DOI: 10.1021/acsabm.3c00826.

(9) Li, Z.; Chu, Z.; Yang, J.; Qian, H.; Xu, J.; Chen, B.; Tian, T.; Chen, H.; Xu, Y.; Wang, F. Immunogenic Cell Death Augmented by Manganese Zinc Sulfide Nanoparticles for Metastatic Melanoma Immunotherapy. *ACS Nano* **2022**, *16* (9), 15471−15483.

(10) Sun, X.; Zhang, Y.; Li, J.; Park, K. S.; Han, K.; Zhou, X.; Xu, Y.; Nam, J.; Xu, J.; Shi, X.; Wei, L.; Lei, Y. L.; Moon, J. J. Amplifying STING activation by cyclic dinucleotide-manganese particles for local and systemic cancer metalloimmunotherapy. *Nat. Nanotechnol.* **2021**, *16* (11), 1260−1270.

(11) Sun, Y.; Yin, Y.; Gong, L.; Liang, Z.; Zhu, C.; Ren, C.; Zheng, N.; Zhang, Q.; Liu, H.; Liu, W.; You, F.; Lu, D.; Lin, Z. Manganese nanodepot augments host immune response against coronavirus. *Nano Res.* **2021**, *14* (5), 1260−1272.

(12) Wang, C.; Sun, Z.; Zhao, C.; Zhang, Z.; Wang, H.; Liu, Y.; Guo, Y.; Zhang, B.; Gu, L.; Yu, Y.; Hu, Y.; Wu, J. Maintaining manganese in

tumor to activate cGAS-STING pathway evokes a robust abscopal antitumor effect. *J. Controlled Release* **2021**, *331*, 480−490.
(13) Ghdeeb, N. J. Effect of Licorice Extract and Manganese Oxide Biosynthesis in the Treatment of Stomach Cancer. *Nano Biomed. Eng.* **2024**, *16* (2), 258.
(14) Zhang, K.; Qi, C.; Cai, K. Manganese-Based Tumor Immunotherapy. *Adv. Mater.* **2023**, *35* (19), No. e2205409.
(15) Wang, C.; Guan, Y.; Lv, M.; Zhang, R.; Guo, Z.; Wei, X.; Du, X.; Yang, J.; Li, T.; Wan, Y.; Su, X.; Huang, X.; Jiang, Z. Manganese Increases the Sensitivity of the cGAS-STING Pathway for Double-Stranded DNA and Is Required for the Host Defense against DNA Viruses. *Immunity* **2018**, *48* (4), 675−687.
(16) Lv, M.; Chen, M.; Zhang, R.; Zhang, W.; Wang, C.; Zhang, Y.; Wei, X.; Guan, Y.; Liu, J.; Feng, K.; Jing, M.; Wang, X.; Liu, Y. C.; Mei, Q.; Han, W.; Jiang, Z. Manganese is critical for antitumor immune responses via cGAS-STING and improves the efficacy of clinical immunotherapy. *Cell Res.* **2020**, *30* (11), 966−979.
(17) Bai, Y.; Li, Y.; Li, Y.; Tian, L. Advanced Biological Applications of Cerium Oxide Nanozymes in Disease Related to Oxidative Damage. *ACS Omega* **2024**, *9* (8), 8601−8614.
(18) Zhou, X.; Wang, Q.; Lei, Z.; Zhang, K.; Zhen, S.; Yao, H.; Zu, Y. Calcium Carbonate-Based Nanoplatforms for Cancer Therapeutics: Current State of Art and Future Breakthroughs. *ACS Omega* **2024**, *9* (11), 12539−12552.
(19) Hu, J. J.; Yuan, L.; Zhang, Y.; Kuang, J.; Song, W.; Lou, X.; Xia, F.; Yoon, J. Photo-Controlled Calcium Overload from Endogenous Sources for Tumor Therapy. *Angew. Chem., Int. Ed.* **2024**, *63* (9), No. e202317578.
(20) Khoshnejad, M.; Parhiz, H.; Shuvaev, V. V.; Dmochowski, I. J.; Muzykantov, V. R. Ferritin-based drug delivery systems: Hybrid nanocarriers for vascular immunotargeting. *J. Controlled Release* **2018**, *282*, 13−24.
(21) Li, L.; Chen, G. Precise Assembly of Proteins and Carbohydrates for Next-Generation Biomaterials. *J. Am. Chem. Soc.* **2022**, *144* (36), 16232−16251.
(22) Song, N.; Zhang, J.; Zhai, J.; Hong, J.; Yuan, C.; Liang, M. Ferritin: A Multifunctional Nanoplatform for Biological Detection, Imaging Diagnosis, and Drug Delivery. *Acc. Chem. Res.* **2021**, *54* (17), 3313−3325.
(23) Fan, K.; Jia, X.; Zhou, M.; Wang, K.; Conde, J.; He, J.; Tian, J.; Yan, X. Ferritin Nanocarrier Traverses the Blood Brain Barrier and Kills Glioma. *ACS Nano* **2018**, *12* (5), 4105−4115.
(24) Liang, M.; Fan, K.; Zhou, M.; Duan, D.; Zheng, J.; Yang, D.; Feng, J.; Yan, X. H-ferritin-nanocaged doxorubicin nanoparticles specifically target and kill tumors with a single-dose injection. *Proc. Natl. Acad. Sci. U.S.A.* **2014**, *111* (41), 14900−14905.
(25) Zhang, S.; Feng, Y.; Meng, M.; Li, Z.; Li, H.; Lin, L.; Xu, C.; Chen, J.; Hao, K.; Tang, Z.; Tian, H.; Chen, X. A generally minimalist strategy of constructing biomineralized high-efficiency personalized nanovaccine combined with immune checkpoint blockade for cancer immunotherapy. *Biomaterials* **2022**, *289*, No. 121794.
(26) Zhang, Z.; Yue, P.; Lu, T.; Wang, Y.; Wei, Y.; Wei, X. Role of lysosomes in physiological activities, diseases, and therapy. *J. Hematol. Oncol.* **2021**, *14* (1), 79.
(27) Kuai, R.; Yuan, W.; Son, S.; Nam, J.; Xu, Y.; Fan, Y.; Schwendeman, A.; Moon, J. J. Elimination of established tumors with nanodisc-based combination chemoimmunotherapy. *Sci. Adv.* **2018**, *4* (4), No. eaao1736.
(28) Reczek, C. R.; Chandel, N. S. ROS-dependent signal transduction. *Curr. Opin. Cell Biol.* **2015**, *33*, 8−13.
(29) Zhang, J.; Simpson, C. M.; Berner, J.; Chong, H. B.; Fang, J.; Ordulu, Z.; Weiss-Sadan, T.; Possemato, A. P.; Harry, S.; Takahashi, M.; Yang, T. Y.; Richter, M.; Patel, H.; Smith, A. E.; Carlin, A. D.; Hubertus de Groot, A. F.; Wolf, K.; Shi, L.; Wei, T. Y.; Dürr, B. R.; Chen, N. J.; Vornbäumen, T.; Wichmann, N. O.; Mahamdeh, M. S.; Pooladanda, V.; Matoba, Y.; Kumar, S.; Kim, E.; Bouberhan, S.; Oliva, E.; Rueda, B. R.; Soberman, R. J.; Bardeesy, N.; Liau, B. B.; Lawrence, M.; Stokes, M. P.; Beausoleil, S. A.; Bar-Peled, L. Systematic identification of anticancer drug targets reveals a nucleus-to-mitochondria ROS-sensing pathway. *Cell* **2023**, *186* (11), 2361−2379.e25.
(30) Zhu, X. J.; Feng, J. Q.; Zheng, M. Z.; Yang, Z. R.; Zhao, L.; Zhang, W.; Zhong, W.; Chen, Y. Y.; Lin, J. Metal-Protein Nanoparticles Facilitate Anti-VSV and H1N1 Viruses Through the Coordinative Actions on Innate Immune Responses and METTL14. *Macromol. Biosci.* **2021**, *21* (4), No. e2000382.
(31) Cheng, Z.; Dai, T.; He, X.; Zhang, Z.; Xie, F.; Wang, S.; Zhang, L.; Zhou, F. The interactions between cGAS-STING pathway and pathogens. *Signal Transduction Targeted Ther.* **2020**, *5* (1), 91.
(32) Samson, N.; Ablasser, A. The cGAS-STING pathway and cancer. *Nat. Cancer* **2022**, *3* (12), 1452−1463.
(33) Ishikawa, H.; Ma, Z.; Barber, G. N. STING regulates intracellular DNA-mediated, type I interferon-dependent innate immunity. *Nature* **2009**, *461* (7265), 788−792.
(34) Kawai, T.; Akira, S. TLR signaling. *Semin. Immunol.* **2007**, *19* (1), 24−32.
(35) Huang, S.; Cheng, A.; Wang, M.; Yin, Z.; Huang, J.; Jia, R. Viruses utilize ubiquitination systems to escape TLR/RLR-mediated innate immunity. *Front. Immunol.* **2022**, *13*, No. 1065211.
(36) Li, Z.; Zhang, X.; Fu, Z.; He, W.; Gao, Y.; Ma, Y. Retinoic acid-inducible gene-1 knockdown induces immature properties in dendritic cells and prolongs the survival time of allograft mice. *Gene* **2024**, *897*, No. 148049.
(37) Liu, S. S.; Bai, T. T.; Que, T. L.; Luo, A.; Liang, Y. X.; Song, Y. X.; Liu, T. Y.; Chen, J. W.; Li, J.; Li, N.; Zhang, Z. C.; Chen, N. N.; Liu, Y.; Zhang, Z. C.; Zhou, Y. L.; Wang, X.; Zhu, Z. B. PI3K/AKT mediated De novo fatty acid synthesis regulates RIG-1/MDA-5-dependent type I IFN responses in BVDV-infected CD8(+)T cells. *Vet. Microbiol.* **2024**, *291*, No. 110034.
(38) Sahoo, B. R. Structure of fish Toll-like receptors (TLR) and NOD-like receptors (NLR). *Int. J. Biol. Macromol.* **2020**, *161*, 1602−1617.
(39) Vidya, M. K.; Kumar, V. G.; Sejian, V.; Bagath, M.; Krishnan, G.; Bhatta, R. Toll-like receptors: Significance, ligands, signaling pathways, and functions in mammals. *Int. Rev. Immunol.* **2018**, *37* (1), 20−36.
(40) Zeng, Q.; Jewell, C. M. Directing toll-like receptor signaling in macrophages to enhance tumor immunotherapy. *Curr. Opin. Biotechnol.* **2019**, *60*, 138−145.
(41) Li, J.; Ren, H.; Qiu, Q.; Yang, X.; Zhang, J.; Zhang, C.; Sun, B.; Lovell, J. F.; Zhang, Y. Manganese Coordination Micelles That Activate Stimulator of Interferon Genes and Capture In Situ Tumor Antigens for Cancer Metalloimmunotherapy. *ACS Nano* **2022**, *16*, 16909−16923, DOI: 10.1021/acsnano.2c06926.
(42) Liang, C.; Xiong, N.; Liu, M.; Chen, Y.; Li, W.; Xu, J.; Sun, Y.; Wang, Y.; Dong, Y.; Fan, W.; Zhang, Y.; Zhang, Z. Manganese immunotherapy for treating osteosarcoma: Glycosylating 1V209 anchored MnO2 nanosheets prompt pro-inflammatory macrophage polarization. *Nano Today* **2023**, *48*, No. 101670.

https://doi.org/10.1021/acsomega.4c06497
ACS Omega 2024, 9, 40226−40233